3D TUMOR SHAPE RECONSTRUCTION FROM 2D BIOLUMINESCENCE IMAGES

Junzhou Huang, Xiaolei Huang, Dimitris Metaxas

CBIM, DCIS,
Rutgers University, NJ, USA

Debarata Banerjee

Cancer Institute of New Jersey,
UMDNJ, NJ, USA

ABSTRACT

This paper introduces a novel and efficient algorithm for reconstructing the 3D shapes of tumors from a set of 2D bioluminescence images which are taken by the same camera but after continually rotating the animal by a small angle. The method is efficient and robust enough to be used for analyzing the repeated imaging of a same animal transplanted with gene marked cells. There are several steps in our algorithm. First, the silhouettes (or boundaries) of the animal and its interior hot spots (corresponding to tumors) are segmented in the set of bioluminescence images. Second, the images are registered according to the projection of the animal rotating axis. Third, the images are mapped onto 3D projection planes and from the viewpoint of each plane, the visual hulls of the animal and its interior tumors are reconstructed. Finally, the intersection of visual hulls from all viewpoints approximates the shape of the animal and its interior tumors. The experimental results show promising performance of our reconstruction method.

1. INTRODUCTION

Bioluminescence imaging (BLI) is an emerging technique for sensitive and noninvasive imaging, which can be used for monitoring molecular events in intact living animals. Important applications of this imaging technique include gene therapy and cell trafficking studies. Unlike fluorescence optical imaging approaches which require an external source of light for excitation of fluorophores, BLI generates a two-dimensional (2D) view of gene expression using a CCD camera based on the internal light produced by luciferases, catalysts in a light generating reaction, through the oxidation of an enzyme-specific substrate (luciferin) [1]. The increasing use of BLI as the choice of small-animal imaging modality is based on the need for repeated imaging of the same animal transplanted with gene marked cells, which is possible using BLI. Other imaging modalities such as mPET, MRI are unsuitable for repeated imaging in a laboratory setting and require sophisticated equipment or allowance for isotope decay to image repeatedly. The problem we tackle in this paper is to recover 3D tumor shape from multiple 2D bioluminescence images of a small animal. There is a need for 3D reconstruction because 2D BLI images do not provide any information on the response in the z-axis(i.e. depth). Recently there has been research work on bioluminescence tomography (BLT) which aims to extract the depth information [2, 3, 4]. However, as shown in [4], this inverse reconstruction problem is ill-posed and in the general case the BLT does not have a unique solution. Furthermore, real systems that implement BLT can be time consuming and not easy to reconstruct the 3D images with high resolution. One potential approach suggested in [3] is to use multiple CCD cameras for simultaneous measurement of bioluminescence signals.

In this paper, we propose a novel and efficient approach to reconstruct 3D tumor shape in small animals using a series of BLI images taken by the same camera but after continually rotating the animal by a small angle. Instead of using multiple cameras, our experimental setup uses a single CCD BLI camera (e.g. IVIS 200 imaging station) to acquire images of an animal at every rotation stage for multiple rotations clockwise around a fixed axis. This set-up is simpler and more flexible than using multiple cameras since we can acquire any number of images by adjusting the rotation angle. Given the multiple BLI images of the animal, we propose to reconstruct the 3D shape of the hot spots (corresponding to tumors) based on a 3D visual hull reconstruction method. Using visual hulls for object shape reconstruction has received extensive attention and has been widely studied over the last decade [5, 6]. The visual hull of an object depends both on the object itself and on the viewing direction, and an exact surface could be constructed if there are sufficient number of viewing directions [7]. Because it is simple and efficient, visual hull is successfully used for many virtual reality application [8].

In this paper, we use visual hulls to reconstruct the shape of tumors captured by a set of BLI images. The proposed method has several steps. First, the silhouettes of objects (e.g. a small animal, or a tumor inside the animal) in all the images are obtained with a simple segmentation approach. Then all the images are registered according to the rotating axis. Finally, the images are mapped onto their respective 3D projection planes, visual hulls generated from all projection directions are generated, and the intersection of all visual hulls are computed to approximate the 3D location and shape of the animal and its interior tumors.

The remainder of the paper is organized as follows. In section 2, we introduce our experimental set up and data ac-

Fig. 1. Examples of BLI images acquired from a small animal with tumor cells growing in the abdomen.

quisition method. Section 3 presents the procedures for segmenting animal tumor silhouettes. Section 4 introduces the method for registering images. The visual hull reconstruction algorithm and experimental results using both a phantom study and real small-animal images are presented in section 5. Section 6 concludes this paper with discussions.

2. SETUP AND IMAGE ACQUISITION

The bioluminescence images were acquired following injection of D-luciferin (given i.p. at 150mg/ml) and image reconstruction was carried out using manufacturer's (the IVIS 100 machine, by Xenogen, Alameda, CA) software. Images were acquired in a standard mode with 2x2 binning. In order to get specificity of the response in the z-axis, we design the following experimental set up.

The animal to be imaged is inserted into a cylindrical 50 ml tube cut at both ends that can be rotated by a small angle (12 degrees) at a time from the vertical axis. Images are acquired at every rotation stage clockwise from the vertical axis. This generates a series of images including the one without any rotation. Fig.1 shows some example BLI images of a mouse with tumor in the abdomen area. The mouse is contained in a 50 ml tube cut at both ends and bottoms. The tumor regions have higher intensity values in the BLI images. The dimensions along long axis and short axis of the mouse tumor is $1.2cm$, $1.1cm$ and $1.1cm$, which is obtained by sacrificing mouse after image capturing.

In the following sections, we also use a set of images from a phantom study (Fig.2(1)). The images were generated by rotating a 50 ml tube clockwise at an increment of 11.25 degrees. Luciferase-positive cell lysates were embedded in agarose inside the tube. The dimensions along long axis and short axis of the cluster of lysates are $1.8cm$, $1.2cm$ and $1.1cm$. It appeared as a hot point in images which were acquired over 20 minutes following injection of D-luciferin.

3. SEGMENTING IMAGES

A visual hull depends both on the object silhouettes and on the camera viewing direction. Before the reconstruction, we should obtain the object silhouettes in the images. In our experiment, as shown in Fig. 2(1), the objects were rotated gradually with a small angle and their bioluminescence images were captured correspondingly. Considering that the images include not only the interested objects (the tube and the tumor), but also the un-interested background, the captured BLI
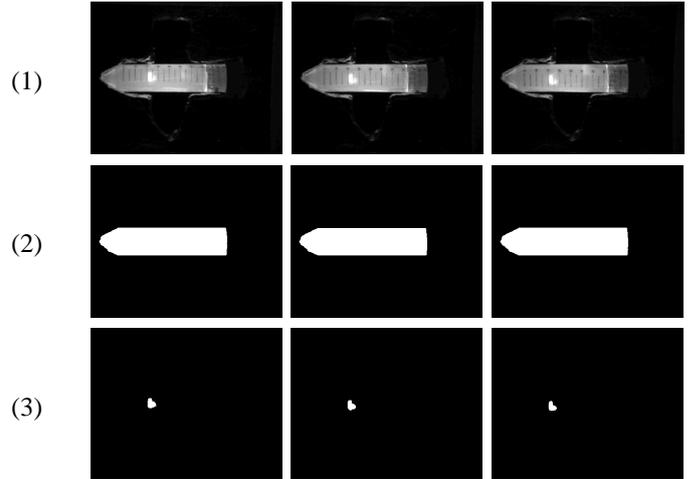
Fig. 2. Segmentation Examples. (1) BLI images. (2) Segmented tubes. (3) Segmented tumors
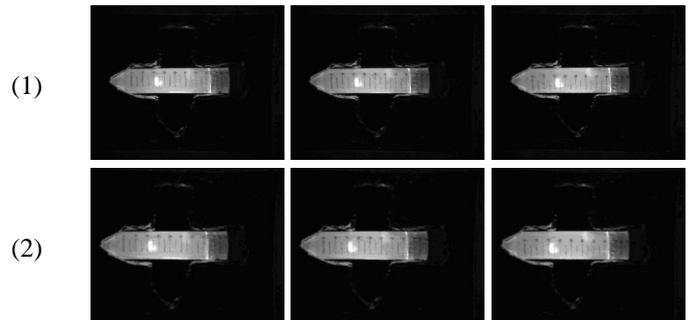
Fig. 3. Registering examples. (1) BLI images. (2) after alignment.

images should be segmented for later processing. In order to facilitate correct segmentation, a monochromatic background was captured to distinguish the tube containing the small animal from the environment in the experiment setup. First, the contour (or silhouette) of the tube containing the small animal is easily extracted from the input images by simple thresholding. Fig. 2(2) shows the tube segmentation result we obtained. Then, according to the characteristic of tumor in the BLI images (they appear as higher intensities), we can segment the tumor from the tube region by combining tumor intensity and edge information. Fig. 2(3) shows segmentation results of the tumor in the images.

4. REGISTERING IMAGES

Due to noise in the imaging system during the rotation of the small animal, the bioluminescence images may not be perfectly aligned. To ensure accurate correspondence across images, we apply an image-based method to register the images such that projections of the rotating axis on all images overlap in the image space. For this purpose, we define an im-

age dissimilarity objective function based on mutual information [9, 10], and recover the translation and rotation parameters by minimizing the objective function. Suppose a source image is f, and its adjacent target image is g. In the most general case, let us consider a sample domain Ω in the image domain of the source image f, we aim to recover the parameters $\mathbf{\Theta} = (T_x, T_y, \theta)$ of a global transformation A such that the mutual information between $f_\Omega = f(\Omega)$ and $g_\Omega^A = g\big(A(\mathbf{\Theta}; \Omega)\big)$ is maximized. Here the parameters T_x and T_y are translation parameters in the x and y directions respectively, and θ denotes the rotation angle. And the definition for such mutual information is:

$$MI(X^{f_\Omega}, X^{g_\Omega^A}) = \mathcal{H}\left[X^{f_\Omega}\right] + \mathcal{H}\left[X^{g_\Omega^A}\right] - \mathcal{H}\left[X^{f_\Omega, g_\Omega^A}\right] \quad (1)$$

In the above formula, X denotes the intensity random variable and $\mathcal{H}$ represents the differential entropy. Then we define the image dissimilarity objective function as:

$$E(A(\mathbf{\Theta})) = -MI(X^{f_\Omega}, X^{g_\Omega^A}) \quad (2)$$

Hence by minimizing this objective function E, we achieve maximizing mutual information. The calculus of variations with a gradient descent method is then used to minimize E and recover the transformation parameters T_x, T_y and θ. Fig. 3(2) shows the registered images. Note that small displacements and rotations between consecutive images are corrected.

5. RECONSTRUCTING 3D TUMOR SHAPE

As introduced above, instead of setting up an image-capturing system with multiple cameras, we take bioluminescence pictures by a single fixed camera while rotating the object (tube or small animal). This setup is equivalent to having multiple cameras surrounding a static object, but it is much simpler and does not require calibrating multiple cameras. Fig. 4 demonstrates the multi-view set up where the planes represent the projection planes for images taken from different views. Since the depth variation due to the object is small compared with the distance between the animal and the camera, changes in the object silhouette along the depth direction are negligible. Thus, an orthographic projection model is reasonable to use in order to reconstruct the 3D object structure and tumor shape. The reconstruction is based on the concept of visual hull. Formally, the visual hull of an object S with respect to the viewing region R, denoted by $VH(S, R)$, is a volume in space such that for each point P in $VH(S, R)$ and each viewpoint V in R, the half-line from V through P contains at least one point of S [5]. This definition simply states that the visual hull consists of all points in space whose images lie within all silhouettes viewed from the viewing region. Stated another way, the visual hull is the maximal object that has the same silhouettes as the original object, as viewed from the viewing region. In our implementation, because we use the orthographic projection model, the segmented object and tumor silhouettes are projected into the 3D space by cylindrical
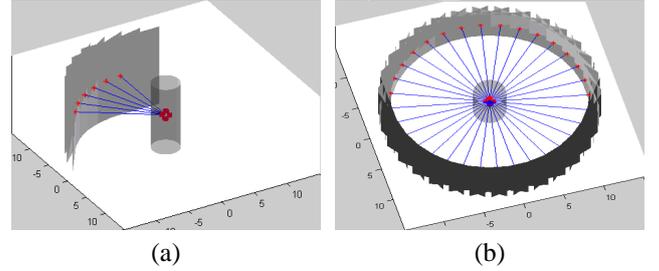
Fig. 4. Setting up projection plane geometry for images taken from different views. (a) some example views for consecutive images. (b) all views forming a full circle.

visual hulls, instead of conical visual hulls in the projective projection model. By computing the intersection of the visual hulls projected from all images (i.e. all viewing directions), we obtain the estimation for the shape and location of the animal and its interior tumors.

5.1. Experimental Results

First, we perform several phantom studies. Fig. 5(a) demonstrates the process of determining the 3D depth of feature points by computing the intersection of 3D rays passing perpendicularly through corresponding feature points on two consecutive images, which are mapped onto their respective projection planes. It shows the reconstructed 3D location of the tube center (the intersection of the two rays in blue) and the 3D location of the tumor center (the intersection of the two rays in red). The tumor centers on the bioluminescence images are computed as the centroids of the high-intensity signal regions (drawn as asterisks on the image planes), and the intersection of 3D rays passing through tumor center locations on images taken from different views gives us the location of the tumor center in 3D. Fig. 5(b) shows the intersection of multiple cylindrical hulls based on the tumor silhouettes. The intersection of all cylindrical hulls gives the 3D reconstruction of the tumor shape. In the phantom study, since the object surface can be approximated using a cylinder, we determine the radius of the cylinder using silhouettes of the tube. Fig. 6 shows the reconstructed 3D tumor viewed in two directions. Fig. 7 shows the reconstructed shape of the tube and tumor, which are viewed in two different directions.

We also do the same procedures to reconstruct animal and tumor shapes from small-animal BLI images. Fig. 8(a-b) shows the reconstructed tumor location and shape from a set of BLI images of the mouse with abdominal tumor.

Based on our approach, we establish the relationship between the reconstructed animal dimension measurements in the animal centered reference frame and that in the physical world. This is achieved by computing the conversion ratio based on one base measurement, such as the diameter or the length of the tube or mouse).
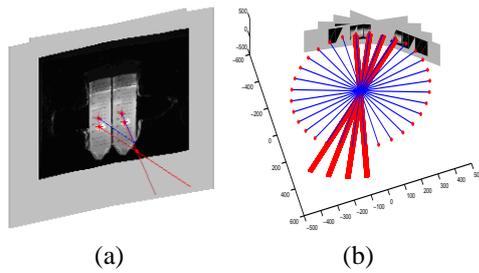
Fig. 5. (a) Line intersection. (b) Cylinder hull intersection.
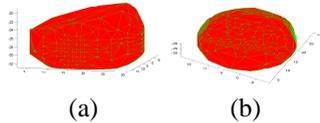
Fig. 6. Reconstructed 3D tumor shape from two views.

5.2. Evaluation

Evaluation of the reconstruction accuracy is done by comparing the recovered 3D shape and location of the tumor with the ground truth in our experimental set up.

In the phantom study, we measured physically the tumor center location, and dimensions along the long axis and short axis of the cluster of luciferase-positive cell lysates that appeared as hot (or bright) spots in the images. Comparing our reconstruction result with the ground truth (Detailed in section 2), the distance in 3D between the measured hot spot center and the reconstructed center is around $2mm$, the difference between the long axis dimensions is less than $1mm$, and the difference between the short axis dimensions is less than $1mm$. For the mouse example, the reconstructed tumor dimensions are all less than $2mm$ different from the true dimensions, and the reconstructed tumor location matches with the ground truth acquired by sacrificing the mouse.

6. DISCUSSIONS AND CONCLUSIONS

We have presented a novel image-based framework for 3D tumor shape reconstruction from a series of 2D bioluminescence images. This is the first image-based BLI reconstruction method presented, to the best of our knowledge, and the simplicity and efficiency of our framework gives it great potential in studying cell trafficking, tumor growth, response to therapy in vivo as well as imaging and analyzing processes such as hematological reconstitution following bone marrow transplantation, among others.

7. REFERENCES

[1] P. Mayer-Kuckuk, L. G. Menon, R. G. Blasberg, J. R. Bertino, and D. Banerjee. Role of reporter gene imaging in molecular and cellular biology. *Biol. Chem.*, 385:353–361, 2004.

[2] X. Gu, Q. Zhang, L. Larcom, and H. Jiang. Three-dimensional bioluminescence tomography with model-based reconstruction. *Optics Express*, 12(17):3996–4000, 2004.

[3] G. Wang, E. A. Hoffman, G. McLennan, L.V. Wang, M. Suter, J. F. Meinel, and et al. Development of the first bioluminescent ct scanner. *Radiology*, 229(P):566, 2003.

[4] G. Wang, Y. Li, and M. Jiang. Uniqueness theorems in bioluminescence tomography. *Med. Phys.*, 31:2289–2299, 2004.

[5] A. Laurentini. The visual hull concept for silhouette-based image understanding. *IEEE Trans. PAMI*, 16(2):150–162, February 1994.

[6] M. Brand, K. Kang, and D. Cooper. Algebraic solution for the visual hull. In *CVPR*, pages 30–35, 2004.

[7] K. Kutulakos and S. Seitz. A theory of shape by space carving. *IJCV*, 1(3):307–314, March 2000.

[8] W. Matusik, C. Buehler, L. McMillan, and S Gortler. Image-based visual hulls. In *SIGGRAPH2000*, pages 187–194, 2000.

[9] F. Maes, A. Collignon, D. Vandermeulen, G. Marchal, and P. Suetens. Multi-modality image registration by maximization of mutual information. *IEEE Transactions on Medical Imaging*, 16(2):187–198, 1997.

[10] P. Viola and W. Wells. Aligment by Maximization of Mutual Information. In *ICCV*, pages 16–23, 1995.

Fig. 7. Reconstructed 3D tumor (red) in the tube (gray) in the phantom study, from two views
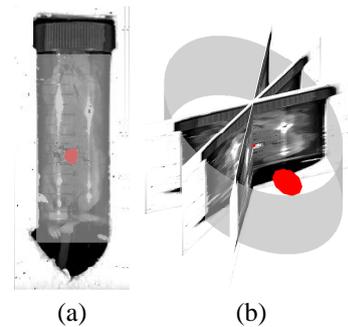
Fig. 8. Reconstructed 3D tumor (red) in the tube (gray) containing the mouse, from two views.